frontiers | Frontiers in Nanotechnology

TYPE Original Research
PUBLISHED 02 February 2024
DOI 10.3389/fnano.2024.1335346

OPEN ACCESS

EDITED BY
Jose Mauro Granjeiro,
National Institute of Metrology, Quality and Technology, Brazil

REVIEWED BY
Iram Maqsood,
University of Maryland, United States
Vadanasundari Vedarethinam,
Cornell University, United States

*CORRESPONDENCE
Mariano J. García-Soto,
mariano.soto@uaslp.mx
Omar González-Ortega,
omar.gonzalez@uaslp.mx
Sergio Rosales-Mendoza,
rosales.s@uaslp.mx

RECEIVED 08 November 2023
ACCEPTED 03 January 2024
PUBLISHED 02 February 2024

CITATION
Farfán-Castro S, García-Soto MJ, Betancourt-Mendiola L, Cervantes J, Segura R, González-Ortega O and Rosales-Mendoza S (2024), Synthesis and evaluation of gold nanoparticles conjugated with five antigenic peptides derived from the spike protein of SARS-CoV-2 for vaccine development. *Front. Nanotechnol.* 6:1335346. doi: 10.3389/fnano.2024.1335346

Synthesis and evaluation of gold nanoparticles conjugated with five antigenic peptides derived from the spike protein of SARS-CoV-2 for vaccine development

Susan Farfán-Castro[1], Mariano J. García-Soto[2]*, Lourdes Betancourt-Mendiola[1,2], Jacquelynne Cervantes[3], René Segura[3], Omar González-Ortega[1,2]* and Sergio Rosales-Mendoza[1,2]*

[1]Sección de Biotecnología, Centro de Investigación en Ciencias de la Salud y Biomedicina, Universidad Autónoma de San Luis Potosí, San Luis Potosí, Mexico, [2]Facultad de Ciencias Químicas, Universidad Autónoma de San Luis Potosí, San Luis Potosí, Mexico, [3]Unidad de Investigación, Facultad de Medicina Veterinaria y Zootecnia, Universidad Nacional Autónoma de México, Ciudad de México, Mexico

Introduction: The development of innovative anti-COVID-19 vaccines is a need to ensure the population's immunity worldwide, with broad protection against variants of concern and low cost as the main goals. Gold nanocarriers are potential entities that could aid in the development of innovative vaccines having thermal stability, high immunogenicity, and safety as the main attributes. Moreover, this approach could lead to adjuvant-free formulations, which will reduce the costs of vaccines.

Methods: In this study, five peptides (P_1, P_2, P_3, P_4, and P_5) corresponding to linear epitopes of the SARS-CoV-2 spike (S) protein were chemisorbed on gold nanoparticles (AuNP) of 20 nm, prefunctionalized with heterobifunctional polyethylene glycol, by using glutaraldehyde as crosslinker to generate nanovaccine prototypes.

Results and discussion: The surface modification was confirmed by DLS with an increase of 31.7 $\pm$ 1.8 nm in the hydrodynamic diameter and an average ζ potential of −8.3 $\pm$ 2.2 mV in PBS (as excipient). The coupling concentration achieved was 23.7 $\pm$ 7.1 µg of peptide per mg AuNP. These AuNP-based conjugates showed no inherent toxicity in assays performed with HEK293T cells, in which a 100–1,000 µg/mL concentration range only led to a temporary decrease of up to 30% in cell viability after 48 h of treatment with restoration by 72 h. The immunogenicity of the conjugates produced was assessed in test mice subjected to three subcutaneous doses at 2-week intervals. Significant levels of IgM against each target peptide were observed at an early stage of the immunization scheme in all groups, reaching maximum levels after the second dose, whereas the IgG response increased after the third dose. The AuNP-P_2, AuNP-P_3, and AuNP-P_5 conjugates induced the highest levels of IgG antibodies, lasting for at least 2 months after the last boost, with a predominance of the IgG1 subclass. Although the magnitude of the response induced by the gold conjugates was

comparable to that with alum as adjuvant, these nanoconjugates induced a longer response. Our data support the use of AuNP as carriers in innovative vaccines against SARS-CoV-2.

KEYWORDS

humoral response, nanovaccine, adjuvant, COVID-19, antigen carrier

1 Introduction

The coronavirus disease 2019 (COVID-19) pandemic, currently recognized as ongoing health issue, has infected almost 676.6 million people worldwide and caused the death of 6.9 million people as of October 2023 (World Health Organization, 2023). The causal agent, SARS-CoV-2, belongs to the family *Betacoronoviridae*, from which other pathogenic strains such as the severe acute respiratory syndrome coronavirus 1 (SARS-CoV-1) and the Middle East respiratory syndrome-related coronavirus (MERS-CoV) caused epidemic outbreaks in 2003 and 2012, respectively (Krishnamoorthy et al., 2020).

The epidemiologic impact of SARS-CoV-2 (Ghafari et al., 2022) led to the accelerated development of vaccines, achieving in a record time the approval for emergency use of several vaccines based on different platforms. These vaccines include mRNA (Moderna and Pfizer-BioNTech), non-replicating viral vectors (Oxford-AstraZeneca), inactivated viruses (Sinovac and Bharat Biotech), and recombinant proteins (Novavax and Sanofi-GSK) as immunogens (Callaway, 2020; Chung et al., 2021).

Since the first reports of SARS-CoV-2 infections in humans, numerous genetically distinct lineages have evolved (CoVariants, 2020). Recently, the emergence of several variants of concern (VOC) bearing mutations with phenotypic implications is of critical interest for the field since VOC exhibit increased transmissibility, enhanced disease severity, or the capability to escape from neutralizing antibodies, which impose the need for modifying the handling strategies of the disease. Its increased transmissibility is of particular concern, as it increases the infection rates and may require more stringent public health measures. Variants escaping from neutralizing antibodies induced by the vaccines originally used require the development of new vaccines updated with the new antigenic sequences (McLean et al., 2022). Moreover, the current vaccines have a low efficacy in terms of protecting against the infection onset and its transmission among individuals. In this context, the development of new vaccines based on rationally designed antigens and mucosal administration (i.e., oral or intranasal routes) is a potential approach to overcome the low protection against infection, transmission, and scape by new variants (Dai and Gao, 2021; European Medicines Agency, 2021; U.S. Food and Drug Administration, 2021).

The typical target in the current COVID-19 vaccines is the spike (S) protein, which is a potent immunogen even in its soluble form, inducing protective cellular and humoral immune responses (Kang et al., 2021). An alternative is the use of synthetic peptides representing epitopes from the S protein, which allows focusing the immune response on the antigenic determinants that mediate protection. However, since peptides are poorly immunogenic, the use of a carrier/adjuvant is crucial. Nanoparticles may act as protective carriers that prolong the half-life of the antigen, exert immunostimulatory activities, and ultimately enhance the immune response. Gold nanoparticles (AuNP) are an advantageous material to use in nanovaccines due to their biocompatibility (Shukla et al., 2005), tunability in terms of surface modification with biomolecules (Bartczak and Kanaras, 2011; Perry et al., 2012; Rahme et al., 2013; Vasquez et al., 2014; Wang et al., 2013), convenient size, and synthesis approach (Mironava et al., 2010; Niikura et al., 2013; Favi et al., 2015). These characteristics offer the potential to favor the development of safe and highly immunogenic vaccines. The feasibility of AuNP-based vaccine prototypes has been assessed with promising results in terms of the induction of humoral and T cell responses (Dykman et al., 2018; Li Y. et al., 2020; Y; Liu et al., 2021; Wang et al., 2017; Zhang, 2015; Zhou et al., 2016). Some studies have reported the induction of Th1 (Climent et al., 2018; Shinchi et al., 2019), Th2, and Th17 responses (Tapia et al., 2021; Trabbic et al., 2021) which indicate that these carriers are versatile entities for the design of a diverse group of vaccines. AuNP have also been shown to be efficiently internalized by dendritic cells leading to their activation, which explain their adjuvant effects (Raghuwanshi et al., 2012; Tomić et al., 2014; Gulla et al., 2019; Meka et al., 2019).

Until now, most of the subunit COVID-19 vaccines are based on the full-length S protein or its receptor-binding domain (RBD) as target antigens. However, exploring epitope-based vaccines formulated with specific peptides is an alternative for the generation of universal vaccines based not necessarily on the RBD, but in linear, conserved epitopes with neutralizing potential (Ng et al., 2022). In this study, five peptides derived from the S protein, spatially distributed in the S1 and S2 subunits (Figure 1) were individually conjugated to AuNP. The methods for the efficient generation of the AuNP conjugates, their physicochemical characterization, and immunogenicity assessment in test mice are reported. Overall, the nanovaccines proposed have the ability of inducing humoral responses against the SARS-CoV-2 spike protein.

2 Materials and methods

2.1 Selection of peptide antigens

Five linear epitopes from the S protein were selected based on a bibliographic search of epitopes with demonstrated antigenicity and potential to generate neutralizing antibodies (Amrun et al., 2020; Heffron et al., 2020; Li L. et al., 2020; Poh et al., 2020; Pinto et al., 2021). These epitopes correspond to antigenic regions derived from the S protein of SARS-CoV-2. The peptide sequences and their position in the S protein are: P_1 (553-TESNKKFLPFQQFGRDIA-570), P_2 (625-HADQLTPTWRVYSTGSNV-642), P_3 (673-SYQTQTNSPRRA-684), P_4 (810-PDPSKRSFIEDLLFNKV-826), and P_5 (1146-DSFKEELDKYFKNHTS-1161). The corresponding peptides were synthesized by GenScript Biotech (Piscataway, NJ).

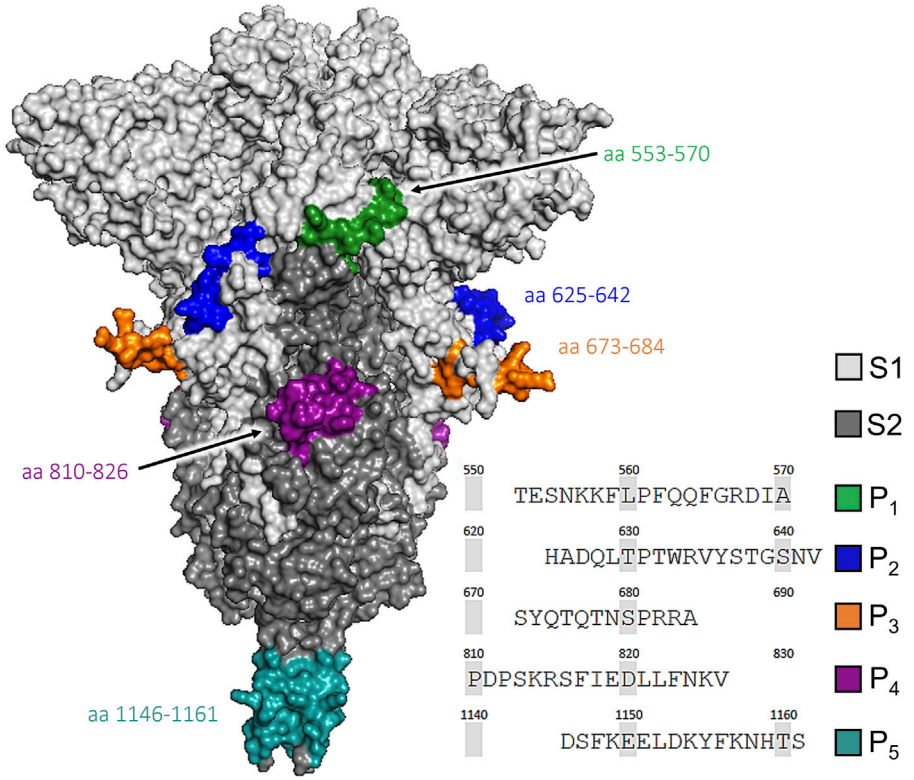

FIGURE 1
Molecular structure of the SARS-CoV-2 spike (S) protein showing its S1 (light grey) and S2 (dark grey) subunits. The locations of the selected peptides sequences are marked as: P_1 (553–570, green), P_2 (625–642, blue), P_3 (673–684, orange), P_4 (810–826, purple), and P_5 (1,146–1,161, teal). The 3D visualization was obtained from NCBI (PDB ID: 6XR8) and rendered with PyMOL 2.5.4 (Schrödinger Inc., New York, NY).

2.2 Synthesis and conjugation of AuNP

The synthesis of AuNP (5× stock) and the conjugation reactions we performed following previously reported methods (Farfán-Castro et al., 2021). 5% stock solutions of $HAuCl_4$ and sodium citrate were prepared 24 h before using them to ensure their complete speciation. For the synthesis, a reaction mixture containing 1% of each precursor was prepared and stored away from light 5 min. This mixture was added rapidly to a flask with boiling water to obtain a 0.05% final concentration and kept under reflux 30 min. The solutions were prepared with milli-Q water and the flask was washed with aqua regia prior to its use.

For the functionalization, per each mL of AuNP the following reagents were added in this order: 5 µL of 1 M HCl, HS-PEG5k-NH_2 (equivalent to five monolayers of PEG per AuNP, considering a grafting density of 2 PEG/nm^2), and 2 µL of 5% Tween 20. This solution was mixed overnight at 4 rpm. The functionalized AuNP were washed twice with 1× PBST (1× PBS with 0.01% Tween 20) with centrifugation steps in between (10 min at 20,000 × *g*). The derivative AuNP-PEG-NH_2 was divided into five equal parts to perform individual conjugation reactions with the target peptides. 100× glutaraldehyde (GTA) was added as amine-reactive crosslinker, reacted 1 h under constant mixing at 4 rpm, and subsequently washed with PBST. Finally, the amount required of the target peptide to form four monolayers per particle was added, reacted overnight under the same conditions, washed before adding 20× $NaBH_4$, reacted for 1 h, and finally washed. Each conjugate was concentrated 20× to a final volume of 1.5 mL. Major reactants, sequence and reaction steps are described in Supplementary Table S1. The synthesis of AuNP, their functionalization with PEG, and their conjugation with peptides was performed in three separate occasions, characterizing their properties and quantifying unbound peptides to validate their monodispersity and dosage (µg peptide per mg AuNP) prior their use in viability and immunogenicity assays.

2.3 Characterization of AuNP and conjugates

The size and morphology of AuNP were analyzed using a transmission electron microscope JEM-2001 (JEOL Ltd., Tokyo, Japan) operated at 200 kV. Of a 1:200 dilution of the AuNP synthesized, 5 µL were deposited on a nickel formvar/carbon-coated grid, allowing it to dry 10 min before storing it in a desiccator for 24 h. From the collected TEM images the size distribution of 700 particles was obtained after calculating shape parameters with ImageJ 1.53e (NIH, Bethesda, MD).

The AuNP were characterized before and after their functionalization and conjugation using a UV-vis spectrophotometer Genesys 50 (Thermo-Fisher, Waltham, MA). Changes in the hydrodynamic diameter (d_H), polydispersity index (PdI), and ζ potential were determined with a Zetasizer Pro

(Malvern Ltd., Malvern, United Kingdom). To compare with the as-prepared AuNP, the functionalized and conjugated AuNP were adjusted to 1.0 of absorbance with 0.1× PBS. A capillary cell DTS1070 (Malvern) was used to measure the ζ potential at 25°C with a RI of 0.18 and absorption of 3.343 for gold (Johnson and Christy, 1972).

FTIR analysis was performed to evidence the functional groups associated with the presence of the peptide coupled onto the AuNP surface. For each sample, an aliquot containing 1 mg of gold was concentrated to a volume of 50 µL, deposited on a non-stick silicone surface, and placed in a desiccator for 24 h. The dry sample was carefully transferred with a fine spatula and the spectra were recorded in the 4,000–400 cm^{-1} region with a total of 254 scans, using an IR spectrometer Nicolet iS10 (Thermo-Fisher) with the Smart iTX ATR sampling accessory.

TGA measurements were performed using a thermogravimetric analyzer TGA-550 (TA Instruments, New Castle, DE). Samples of citrate-capped, functionalized, or conjugated AuNP were dried in the same manner as for the FTIR analysis, concentrating an aliquot containing 3 mg of gold in 50 µL. The heating rate was set to 10°C/min with a temperature range of 30–600°C. Pure samples of sodium citrate and HS-PEG5K-NH_2 were analyzed to identify the signals corresponding to the nanoparticle stabilizer (Supplementary Figures S2–S5).

2.4 Analysis of remanent peptides by HPLC

The unbound peptide was quantified from the reaction supernatants by HPLC using an Agilent 1200 Series Gradient (Agilent Technologies, Santa Clara, CA). The separation was carried out on a C18 reversed-phase column with a linear gradient (solution A: 0.1% $C_2HF_3O_2$ in water, solution B: 0.1% $C_2HF_3O_2$ in CH_3CN) at a flow rate of 0.6 mL/min for 10 min. The injection volume was 50 µL at an injection rate of 0.2 mL/min. The detection wavelength was set to 214 nm. Calibration lines for each peptide were prepared with standard solutions in a range of 25–200 µg/mL (Supplementary Figure S1). Each standard and sample were centrifuged 2 min at 21,000 × *g* and the upper phase was recovered and transferred to a vial for HPLC analysis. Unreacted peptide controls were used for each determination at the same initial concentration used for conjugation.

2.5 Resazurin cell viability assay

The cytotoxicity of the conjugates was evaluated in HEK-293T cells (ATCC CRL-3216, USA) using the resazurin reduction assay. Cells were cultured in DMEM (supplemented with 1% penicillin/streptomycin and 10% fetal bovine serum, at 37°C and 5% CO_2) using T75 flasks until reaching 80% confluency. One day before the cytotoxicity evaluation and after over 10 passages, 1×10^4 cells were seeded by triplicate in a 96-well culture plate. Control cells were treated with H_2O_2 (40 mM) or the vehicle alone (RPMI medium). Cells were exposed to different concentrations (0.1–1,000 µg/mL) of functionalized gold nanoparticles (AuNP-PEG-NH_2) or a mixture of the five conjugates (AuNP-mpS) for 24, 48, and 72 h under the culture conditions mentioned above. To evaluate metabolic activity, the cells were exposed to 30 µg/mL of resazurin for 3 h and the fluorescence was recorded (560 nm/590 nm) in a microplate reader FlexStation II (Molecular Devices, San Jose, CA).

2.6 Immunogenicity assessment

Female BALB/c mice experimental groups (8–10 weeks old, n = 5) were randomly established and assigned to one of the following treatments: mixture of the five target peptides (mpS) with $Al(OH)_3$ adjuvant (AH) at low dose (AH mpS L, 5 µg of each peptide) or high dose (AH mpS H, 15 µg of each peptide), peptides in PBST (5 µg of each peptide) or the AuNP-PEG-peptide conjugates, hereafter identified as AuNP-P_1, AuNP-P_2, AuNP-P_3, AuNP-P_4, AuNP-P_5 (corresponding to 5 µg of the target peptide). Four subcutaneous doses (100 µL of total volume) were administered at 2-week intervals (days 1, 15, 30, and 45). Blood samples were collected by tail puncture on days 0, 14, 29, 44, 59 and 104 (Figure 8A). Sera were separated by centrifuging 10 min at 1,200 × *g* and stored at −20°C until further analysis.

2.7 IgG and IgM ELISA analysis

96-well polystyrene plates were coated with each peptide for individual conjugate groups (150 ng/well), a peptide mix for the AH groups (500 ng/well), or with recombinant S protein (200 ng/well, Sino Biological Inc., 40,589-V08H4) diluted in 0.2 M carbonate buffer (pH = 9.6) and incubated overnight at 4°C. Three washes with 0.05% PBST were performed after each incubation. The plates were blocked with a 5% fat-free milk solution at room temperature for 2 h. Serial dilutions of the test sera were applied by triplicate and incubated overnight at 4°C. For secondary labeling, anti-mouse antibodies (IgM, IgG, IgG1, or IgG2a) conjugated with horseradish peroxidase were added and incubated for 2 h at 25°C. Detection was performed by adding ABTS and H_2O_2 as substrate and the optical density was recorded at 405 nm for 1 h using a microplate photometer Multiskan FC (Thermo-Fisher).

2.8 Flow cytometry

The effect of gold conjugates on the maturation of DC2.4 dendritic cells was assessed by flow cytometry. First, 3×10^6 cells were seeded in 2 mL of complete RPMI medium (supplemented with 1% penicillin/streptomycin, 1% MEM non-essential amino acids solution, 10 mM HEPES, 1 mM β-mercaptoethanol, 2 mM L-glutamine, and 2% FBS) in Petri dishes of 60 mm, which were incubated at 37°C with 5% CO_2 for 24 h before adding the conjugates. The cells were washed once with 1× PBS and treated with AuNP-PEG-NH_2 (50 µg/mL), LPS (100 ng/mL), or complete RPMI medium as the control for 24 h. The DC2.4 cells were washed, harvested in 1× PBS supplemented with 5% FBS, and the concentration adjusted to 5×10^5 cells per well.

The CD16 and CD32 Fc receptors were blocked in all samples with 25 µL of anti-CD16/32 for 30 min on ice, washed twice by centrifugation (5 min at 1,200 rpm and 4°C) and immunostained for 25 min with the selected antibodies. Finally, the cells were washed once,

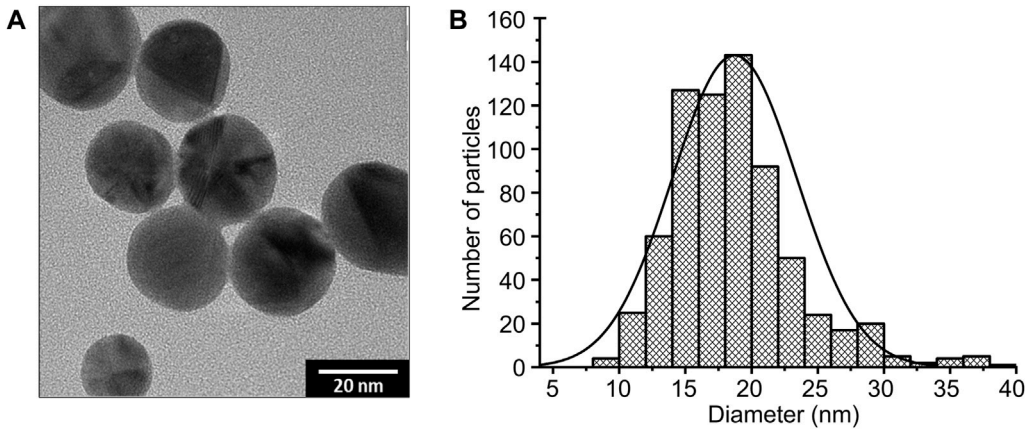

FIGURE 2
Transmission electron microscopy (TEM) image of AuNP at 200 kV **(A)**. Size distribution histogram including a Gaussian fit curve of 700 nanoparticles measured **(B)**.

resuspended in fixative 1% buffered formalin, and stored at 4°C. Throughout the process, the cells were kept on ice and protected from light exposure. The antibodies and their isotype controls used were the following: isothiocyanate (FITC)-conjugated anti-CD11c (FITC Armenian Hamster IgG isotype control), phycoerythrin (PE)-conjugated anti-CD86 (PE Rat IgG2a isotype control), allophycocyanin (APC)-conjugated anti-CD40 (APC Rat IgG2b isotype control), and streptavidin-PerCP/Cyanine5.5 (PerCP/Cyanine5.5 Armenian Hamster IgG isotype control)-conjugated with biotin anti-MHC class II (Biotin Rat IgG2b isotype control). Data were acquired in an Attune Nxt flow cytometer (Thermo-Fisher) and analyzed with FlowJo v.10 (BD Biosciences, Ashland, OR).

2.9 Statistical analysis

The statistical significance was determined using analysis of variance (ANOVA) and Tukey's *post hoc* test. Differences were considered significant when *p*-values were <0.05 and the level of significance is indicated in the figure legends as $*p < 0.05$, $**p < 0.01$, and $***p < 0.001$. The analysis was performed with OriginPro 2021 (OriginLab Corp, Northampton, MA).

3 Results

3.1 Morphological and physicochemical properties of gold conjugates

TEM imaging of 700 nanoparticles confirmed the spherical morphology of the AuNP synthesized with a diameter of 18.70 ± 4.70 nm (Figure 2). The visible absorption spectrum of these as-prepared, citrate-capped AuNP exhibited a maximum absorption signal at 520 nm (λ_{max}), corresponding to the surface plasmon resonance characteristic of spherical nanoparticles of 20 nm (Haiss et al., 2007; Cheng et al., 2020). The analysis by DLS of these AuNP resulted in a d_H and ζ potential values of 20.14 nm and −30.20 mV, respectively.

Once functionalized as AuNP-PEG-NH_2 and conjugated as AuNP-PEG-peptide, hereafter expressed as AuNP-PEG and AuNP-P_i (i = 1, . . ., 5), their main absorption signals red-shifted 1–2 nm, while their signal distribution remained similar (broadened only 2 nm with PEG), when comparing the normalized visible spectra (Vis) of both with that of AuNP. Moreover, their maximum absorbance remained at 1.02 ± 0.07, in range with that of AuNP (≈1), while none exhibited secondary signals at longer wavelengths that would clearly indicate aggregation (Figure 3A).

The conjugation of peptides on PEG-functionalized AuNP was proven by tracking changes in their d_H and ζ potential. These measurements evidenced AuNP with d_H increased 21.7 and 31.7 ± 1.8 nm once pegylated and then conjugated, respectively; with polydispersity indexes (PdI) of 0.2 ± 0.04, consistent with suspensions having monodisperse size distributions. Moreover, none of the suspensions exhibited additional signals in the μm range that would correspond to aggregates (Figure 3B).

Compared to unmodified AuNP, the ζ potential of AuNP-PEG-NH_2 became less negative (attributed to the amino groups from PEG), reaching a value of −6.39 mV in PBS (pH 7.4), while that of the conjugates ranged from −11.70 to −5.87 mV in the same buffer. Overall, the data confirmed changes in the surface of AuNP.

3.2 FTIR characterization

To confirm the nature of the coating on the gold nanoparticles after each modification, FTIR analysis was performed on desiccated samples (Figure 4). The FTIR spectrum of citrate-capped AuNP showed a broad band characteristic of O–H stretching in the 3,657–3,000 cm^{-1} range (1) and another at 1,415 cm^{-1} corresponding to COO^- symmetric stretching (10), in addition to two bands between 2,912–2,845 cm^{-1} of C–H asymmetric (3) and symmetric (4) stretching. AuNP-PEG-NH_2 showed additional bands to those of citrate-capped AuNP that confirmed surface ligand exchange. The main bands correspond to the C–N stretching of amine I at 1257cm^{-1} (12), C–O stretching of the

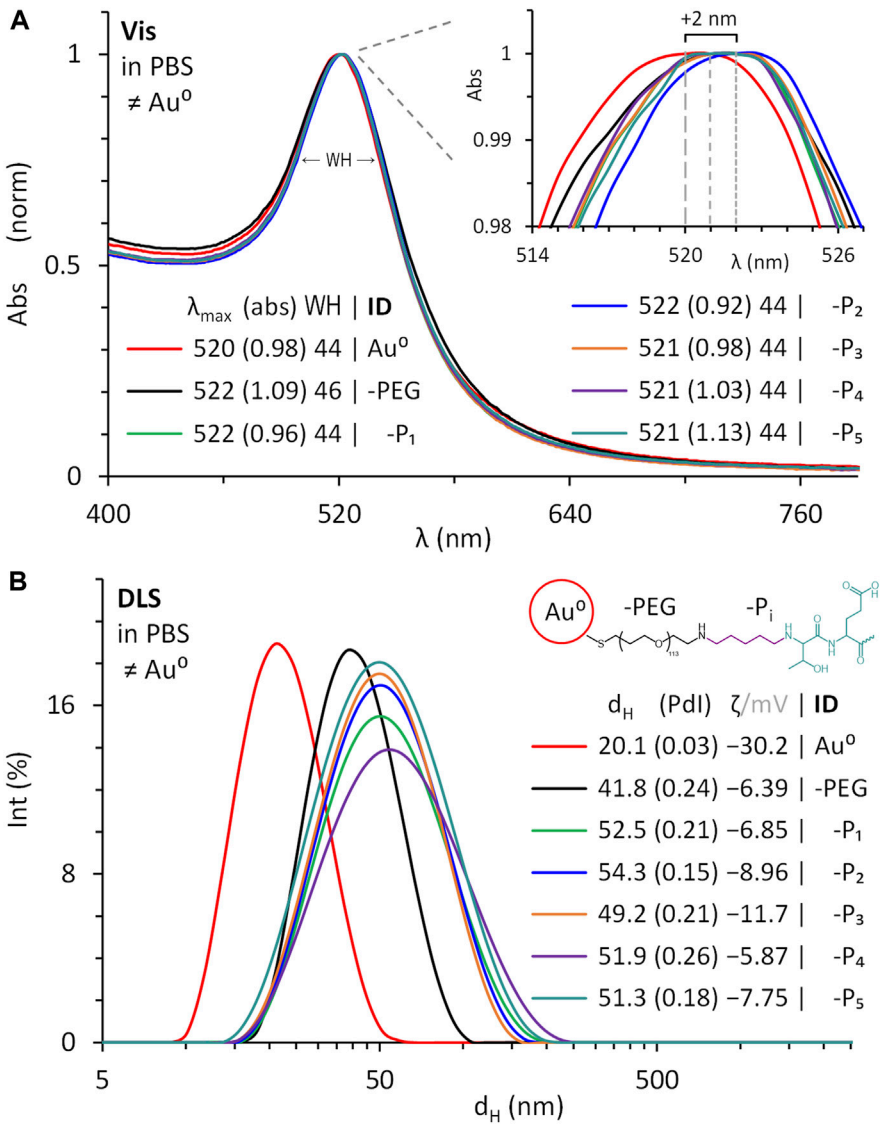

FIGURE 3
Normalized visible spectra **(A)** and dynamic light scattering **(B)** of as-prepared citrate-capped AuNP (Au^0), compared to the functionalized with thiol-polyethylene glycol (PEG)-amine, and conjugated with the peptides selected (P_1 to P_5) in PBS. Absorbance (abs) at λ_{max}, full-width at half-maximum (WH), hydrodynamic diameter (d_H), polydispersity index (PdI), and ζ potential at pH 6 for Au^0 and pH 7.4 for the reacted and suspended in PBS.

ether groups between 1,084–1,020 cm^{-1} (14 and 15), and the C–H rocking band at 720 cm^{-1} (18), known as the CH_2 long-chain band. It is important to note that the S–Au dative bond formation was consolidated with a small band at 451 cm^{-1} (19) and the S–C stretching of the polyethylene glycol polymer chain was localized with a sharp band at 794 cm^{-1} (17). Finally, for AuNP-PEG-P_i the bands at 1725 and 1,622 cm^{-1} (5 and 6) correspond to C=O stretching of carboxylic acid and amide II, as well as at 1,576 and 1,543 cm^{-1} (7 and 8) for N–H bending of amine I and amide II, respectively, which validated the presence of conjugated peptides. Other bands found only in the gold conjugates were C–H bending of the methylene group (1,465 cm^{-1}, 9), O–H bending of carboxylic acids (1,140 cm^{-1}, 13) and phenol from the amino acid tyrosine present in the conjugates P_2, P_3, and P_5 (1,333 cm^{-1}, 11). Furthermore, amino acids exhibited a strong broad O–H band in the 3,660–3,000 cm^{-1} region due to the carboxylic acid and alcohols from amino acids such as serine, threonine, and tyrosine.

3.3 TGA characterization

The observed weight lost below 200°C was attributed to the evaporation of residual water in the sample and only the weight changes registered above 200°C were considered as part of the organic components of it. The thermogram for pure sodium citrate showed three mass losses, one of which was attributed to the partial degradation of sodium citrate at around 310°C and its residues at 450°C (Supplementary Figure S4) (Marcilla et al., 2018; F; Liu et al., 2018). The thermogram for pure HS-PEG5K-NH_2 showed a derivative peak at 380°C (Supplementary Figure S5) with a weight

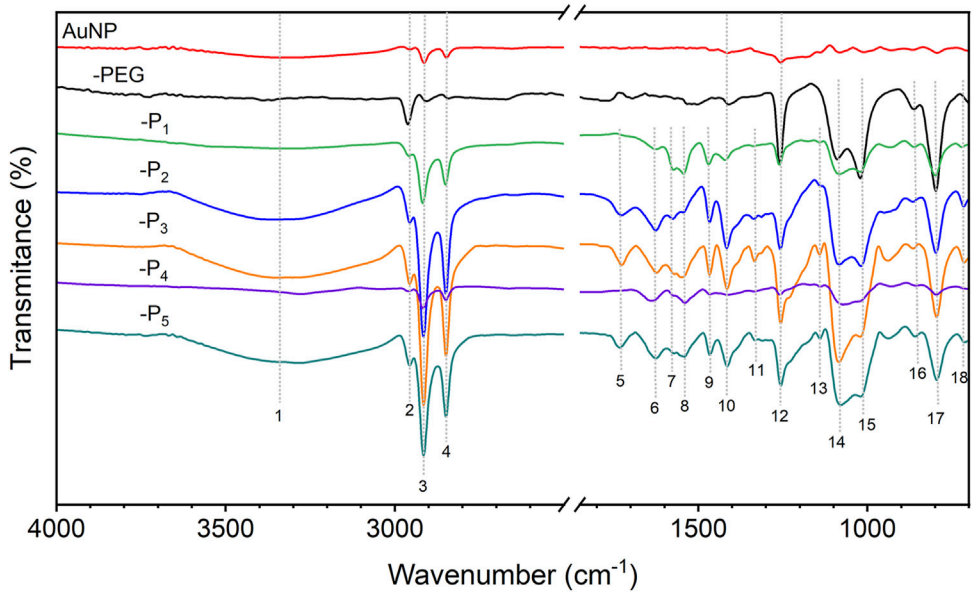

FIGURE 4
FTIR spectra of citrate-capped AuNP (Au^0), after being functionalized with thiol-polyethylene glycol (PEG)-amine, and conjugated with peptides (P_1 to P_5). The functional group assigned to each band number is in Supplementary Table S2.

loss of 96.5%, similar to that of the functionalized and conjugated AuNP. Derivative peaks were also found around 350°C and 400°C, coinciding with references that attribute this mass loss to the decomposition of PEG (Qian et al., 2017; Lu et al., 2019).

As shown in Figure 5, the citrate-capped AuNP had a weight loss of 0.99% at the end of the analysis, while for the PEG-functionalized AuNP the loss of organic material was notably higher. Considering the TGA signal changes, the PEG content in the sample is 8.3%, while in the conjugates is 7.18% ± 0.98%. These weight fractions were useful to calculate the grafting density (σ_{TGA}) as reported before (Das et al., 2016), which was estimated at 0.62 ± 0.09 molecules/nm^2 (Supplementary Table S3). The weight loss of organic material in the gold conjugates, from 200°C to 600°C, was 12.44% ± 0.7% (0.36 ± 0.09 mg), of which 5.26% ± 1.2% (0.15 ± 0.01 mg) corresponds to the conjugated peptide (Supplementary Table S4). Since the amount of peptide monolayers in the conjugates was 1.14 ± 0.25 (HPLC analysis), this data was used to compare the amount of peptide bound to the AuNP according to the mass of peptide added to the conjugation reaction (theoretical), against the weight of peptide lost in the conjugates analyzed by TGA. Theoretically, 0.12 ± 0.02 mg of peptide would have to be found in the gold conjugates and the thermogravimetric analysis indicated that there is actually 0.15 ± 0.01 mg (Supplementary Table S5). This result supports the success of the conjugation strategy since the difference between both estimates is marginal.

3.4 Determination of bound peptide

To determine the amount of bound peptide in each conjugate, the supernatants containing unbound peptide in the conjugation reactions were recovered and analyzed by reverse-phase HPLC. Multiple peak signals with different retention times were found in the chromatograms of supernatants P_1 (four), P_3 (three), and P_2 (two) that could be attributed to the amount of reactive primary amines in their amino acid sequence (8, 8, and 5 primary amines, respectively), which could cross-link GTA (Figure 6). The concentration of each unbound peptide was calculated by interpolation with the corresponding calibration line (Supplementary Figure S1) and subtracted from the concentration measured in the unreacted controls with the same initial concentration to determine the amount of peptide bound or remaining in the colloidal suspension (Supplementary Table S5). The concentration of bound peptide was 47.3 ± 14.2 μg/mL in freshly prepared conjugate suspensions with 2 mg/mL of AuNP. Considering 1 mg of Au^0, from original suspensions of AuNP concentrated 20×, the amount of peptide chemisorbed per mass of AuNP is 23.7 ± 7.1 μg/mg P_i/Au^0.

3.5 Cytotoxicity assay

To test whether AuNP are toxic at the cellular level, a HEK-293T cell line was exposed to a range of AuNP concentrations. Cellular cytotoxicity was measured at 24, 48, and 72 h of stimulation by measuring the metabolic activity of living cells, using the resazurin reduction method. The results showed that there is no significant difference between AuNP-PEG and AuNP-mpS regardless of the material concentration ($p > 0.05$; Figure 7). After 24 h of incubation with the functionalized nanoparticles, a slight decrease in metabolic activity was observed from 100 μg/mL. However, this effect was not significant. Remarkably, 48 h after adding the stimulus there was a statistically significant decrease of cell viability from 100 μg/mL of AuNP-PEG and 250 μg/mL of AuNP-mpS ($p < 0.05$), which might suggest a higher toxicity for AuNP-PEG. However, for the treatment at the higher concentration (1,000 μg/mL) evaluated at 72 h post-

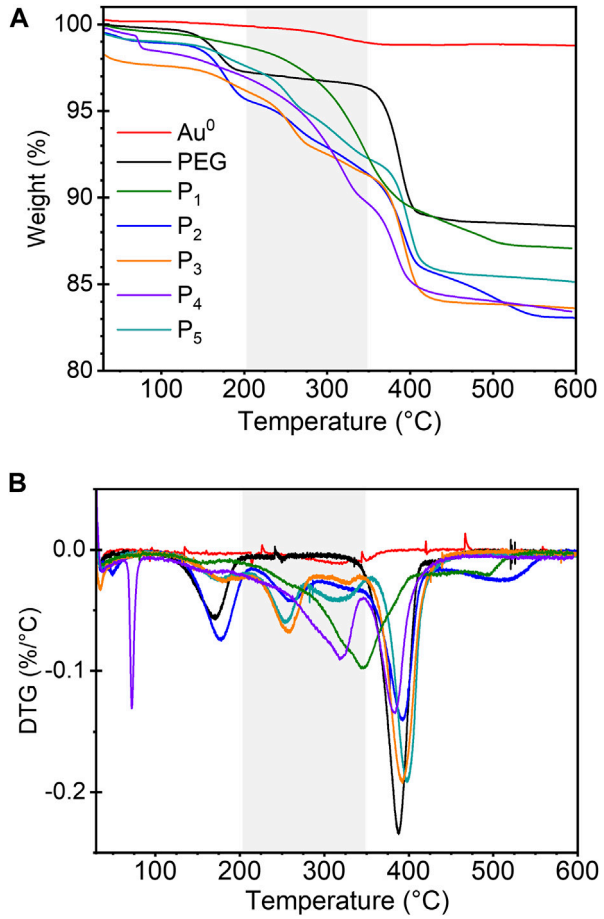

FIGURE 5
TGA **(A)** and DTG **(B)** plots of citrate-capped AuNP (Au^0), functionalized with thiol-polyethylene glycol (PEG)-amine, and conjugated with peptides (P_1 to P_5). The gray vertical band corresponds to the temperature range in which the mass loss due to the decomposition of peptides was identified.

exposure, the values for AuNP-PEG were higher (mean value: 71%) respect AuNP-mpS (mean value: 64%); therefore no consistent trend was observed for the viability decrement induced by the test materials. Moreover, after 72 h of stimulation, cell viability was recovered with both treatments, up to 87% with AuNP-PEG and 91% with AuNP-mpS at the highest concentration added, reaching values that were not statistically different respect the control ($p > 0.05$). Therefore, the general pattern observed for the metabolic activity of the cells exposed to either AuNP-PEG or AuNP-mpS comprised a transient negative effect on the metabolic activity at the 48 h post-exposure with a restoration at the normal levels at 72 h post-exposure, which justified the *in vivo* evaluation of AuNP-mpS as such nanomaterials were not found to be inherently toxic.

3.6 Immune response induced by AuNP conjugates in mice

The ability of the proposed AuNP-PEG-peptide conjugates to increase the immunogenicity of each peptide was tested by immunizing mice with individual conjugates and comparing the induced humoral response to that attained in a group treated with the cocktail of peptides adjuvanted with alum (HA). ELISA data revealed that IgM induction occurred after priming, reaching maximum levels after boosting (day 30), followed by a remarkable decrease (Figure 8B). In contrast, the IgG response was triggered after the third dose with either conjugate or peptides in alum, reaching its maximum levels on day 45 (Figure 8C). Mice that received the high dose of peptides in alum produced significantly higher levels of anti-mpS IgM than the mice in the low dose group, but the IgG levels did not show a dose-dependent effect ($p < 0.05$).

It is important to note that the AuNP-P_2, AuNP-P_3, and AuNP-P_5 conjugates induced the highest concentration of IgG antibodies, which lasted for up to 2 months after the last immunization (Figure 8C, $p < 0.001$). The mice immunized with the AuNP-P_2, AuNP-P_3, and AuNP-P_5 conjugates reached significantly higher IgG antibody titers with respect to the other groups (namely, AuNP-P_1, AuNP-P_4 and HA groups at two dose levels, Figure 9A), with an IgG1 subclass predominancy over IgG2a (Figure 9B).

To evidence the ability of the antibodies induced by the conjugates to recognize the native target (S protein), ELISA was performed using the recombinant full length S protein as target antigen. The results showed an IgG antibodies titer induced by AuNP-P_1 that was 8-fold higher than that obtained against P_1. In this case, the antibodies induced by the AuNP-P_2, AuNP-P_3, and AuNP-P_5 conjugates revealed lower titers than those obtained against the respective peptide and did not represent a statistically significant difference with respect to AuNP-P_4 and high-dose AH (Figure 9C).

3.7 Maturation of dendritic cells

The effect of the functionalized AuNP on dendritic cell maturation was evaluated by flow cytometry of DC2.4 cells stimulated for 24 h with 50 μg/mL of AuNP-PEG-NH_2. Compared against control cells treated with vehicle only, the AuNP were found to induce cell maturation by enhancing the expression of the costimulatory molecule CD86, whereas the CD40 expression was decreased (Figure 10).

4 Discussion

Aluminum hydroxides are by far the most used adjuvants in vaccines in part due to their low cost and the fact that are patent-free (Shardlow et al., 2018). However, several studies have shown that this type of adjuvants do not induce long-lasting immune responses against SARS-CoV-2. In the present study, AuNP-based conjugates targeting peptides from SARS-CoV-2 were synthesized and characterized *in vitro* and *in vivo* as an effort to trigger the development of innovative nanovaccines against COVID-19, not depending on conventional adjuvants that tend to be poorly effective or those with patents that restricts their use in developing countries. Overall, the synthesis and conjugation approach followed to obtain the AuNP-peptide conjugates were efficient, allowing to obtain conjugates with enough antigen concentration for *in vitro* and *in vivo* evaluations. The use of heterobifunctional HS-PEG5k-NH_2

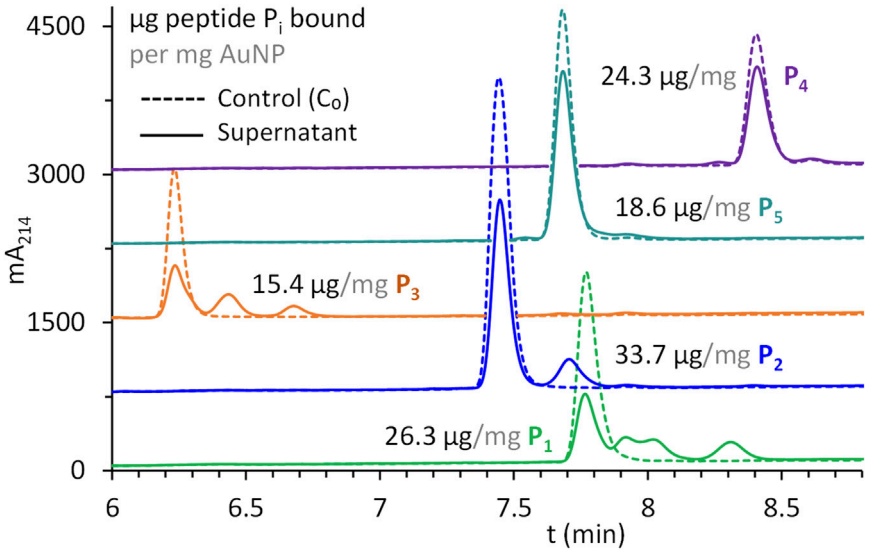

FIGURE 6
Peptides P_1 to P_5 quantified by HPLC from supernatants recovered after their conjugation with AuNP and compared to unreacted peptides at the same initial concentration (C_0). Amount of peptide bound calculated as μg of peptide per mg of AuNP from absorbance values at 214 nm.

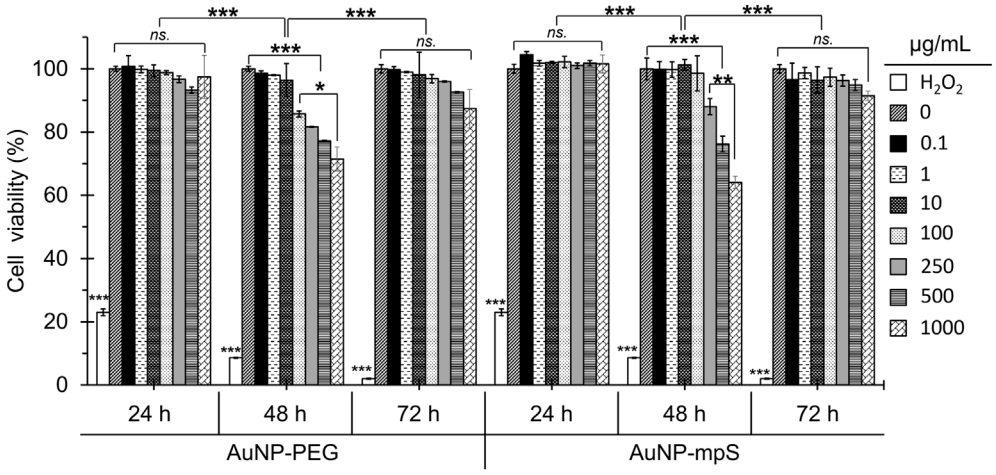

FIGURE 7
Toxicity assessment of the mix of AuNP-peptide conjugates (AuNP-mpS) and AuNP functionalized with thiol-polyethylene glycol-amine (AuNP-PEG). The viability of HEK293-T cells treated at different time intervals was analyzed by the resazurin reduction. Only the 24 h treatment with AuNP-PEG and AuNP-mpS induced a significant decrease in cell viability, reaching 64% and 71%, respectively, with 1,000 μg/mL. No differences in cell viability were found between cells treated with conjugated or functionalized AuNP. Significance values were determined using two-way ANOVA with Turkey test. Significant differences are indicated as *$p < 0.05$, **$p < 0.01$, ***$p < 0.001$, and non-significant differences as *ns*.

facilitated the conjugation of peptides by activating the amino-terminal group with GTA. This *bis*-aldehyde crosslinker is widely used for the reactivity of the aldehyde group with primary or secondary amines in proteins, which produces a stable secondary amine and leaves an exposed aldehyde group for subsequent reductive amination reactions (Hermanson, 2013). The reaction induces the formation of Schiff bases, for which reductants such as $NaBH_4$ are used, allowing the stabilization of secondary amine bonds (Ibrahim et al., 2018). The sequence of amino acids in proteins and peptides can have effects on the reactivity of GTA, mainly in short peptides. The peptides used in this work contain amino acids with amino groups in ionizable side chains that are strong nucleophiles in addition reactions. In the chromatograms of conjugation supernatants, peptides P_1, P_2, and P_3 exhibited multiple signals at different retention times which, as mentioned above, may be associated to their amino acid sequence. For example, P_1 and P_3 showed four and three signals, respectively, and are the peptides that contain the highest number of reactive amines, followed by P_2 with two reactive amines and two signals in their chromatogram. Particularly, P_1 contains two contiguous lysine residues that,

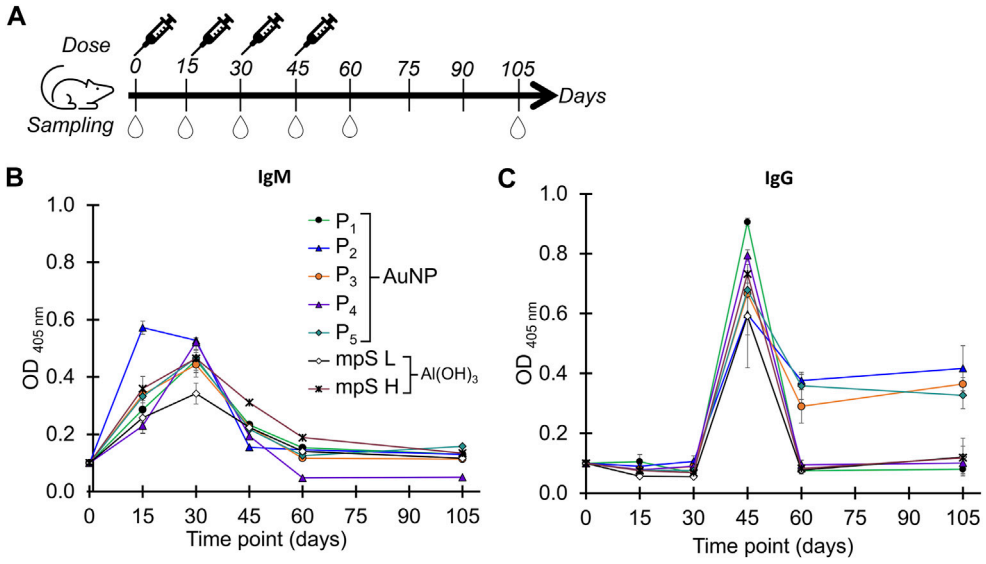

FIGURE 8
Immunogenicity assessment. Immunization scheme **(A)**: 5 female BALB/c mice per group were immunized with each individual gold conjugate (AuNP-P_1 to AuNP-P_5) or a mixture of the five peptides in aluminum hydroxide adjuvant (AH mpS). Mice received four doses s. c. at 2-week intervals, and peripheral blood samples were obtained 1 day before each immunization, 2 weeks (day 60), or 2 months (day 105) after the last immunization. Serum levels of IgM **(B)** and IgG **(C)** antibodies induced in mice immunized with the conjugates or with adjuvant, determined by ELISA at a 1:200 dilution.

when reacted with a cyclic form of GTA (aldol), can form quaternary pyridinium compounds, as well as a powerful nucleophile such as arginine. P_3 contains two contiguous arginine residues in its structure and P_2 contains one residue, but neither contains lysine. Although P_5 and P_4 have three and two lysine residues widely distributed in their sequence, respectively, their chromatogram showed a single peak with no apparent by-product formation between the unbound peptide and the remaining GTA in solution.

Comparable to citrate-capped AuNP, the pegylated and peptide-conjugated AuNP have analogous stability characteristics considering the similarity of their absorption signals and size distributions. The less negative ζ potentials of AuNP-PEG (−6.4 mV) and AuNP-P_i (−8.3 ± 2.2 mV) are due to the adsorption of phosphate anions after washing and resuspending in PBS, a buffer used as excipient for both in cytotoxicity and immunogenicity assays. The stability of the conjugates is remarkable considering that in the herein proposed chemisorption of peptides on AuNP their surface properties change after reacting them sequentially with i) HS-PEG5k-NH_2, ii) GTA, and iii) one of five different peptides (1912 ± 286 Da), with washing cycles consisting of centrifugation and resuspension in 1× PBS, and finally concentrated; 20× for biological assays and 100× for physical-chemical characterization. Considering that after GTA activation the amount of peptide equivalent to four monolayers was added, the bound fraction was expected to correspond to one monolayer of peptide on the polyethylene glycol coating. Therefore, unreacted (soluble) peptide controls analyzed by HPLC were prepared at the concentration of four monolayers. This analysis made it possible to demonstrate that the amount of peptide conjugated to the gold nanoparticles corresponds to 1.14 ± 0.25 monolayers, equivalent to 23.7 ± 7.1 μg/mg.

The density of PEG influences the conformation it acquires on the surface of the nanoparticles and defines the degree of interaction with circulating proteins, by increasing the density of PEG, the degree of interaction with serum proteins and the clearance of the nanomaterial by the mononuclear phagocytic system decreases (Escareno et al., 2018). In a similar PEGylation of AuNP of 20 nm reported with HS-PEG5k-NH_2 the d_H increased 26 nm, with PEG/AuNP molar ratios starting at 500, finding that only the AuNP-PEG from molar ratios starting from 300 and up to 2000 could be centrifuged and resuspended in water (Chen et al., 2013). In our study, the amount of basically the same heterobifunctional PEG to coat one monolayer on AuNP was calculated, corresponding to a molar ratio of 900 compared to the recently consulted reference, adding five times in excess to secure a brush conformation in order to obtain more primary amino groups available on the surface for the subsequent reaction steps. It is known that the relationship between the radius occupied by a PEG chain, known as the Flory radius (R_F), and the distance between the PEG chains (D) allows to estimate of the conformation that PEG molecules acquire on the surface of nanoparticles (Cruje and Chithrani, 2014; Maurel et al., 2021). In this work, the R_F/D ratio has a value of 4.11, indicating that the PEG chains acquire a brush conformation in both functionalized AuNP and conjugates.

It has been documented that the functionalization of AuNP with polyethylene glycol improves the biocompatibility of the nanomaterial and optimizes the cell internalization (Foroozandeh and Aziz, 2018; Bekić et al., 2019). The resazurin assay revealed that both conjugated and functionalized nanoparticles had no toxic effect on HEK293T cells in a 0.1–1,000 μg/mL range after 24 and 72 h of treatment. However, the nanomaterial reduced the cell viability up to 30–40% after 48 h of treatment from 100 μg/mL onwards, but this activity was normalized 24 h later. This behavior is consistent with

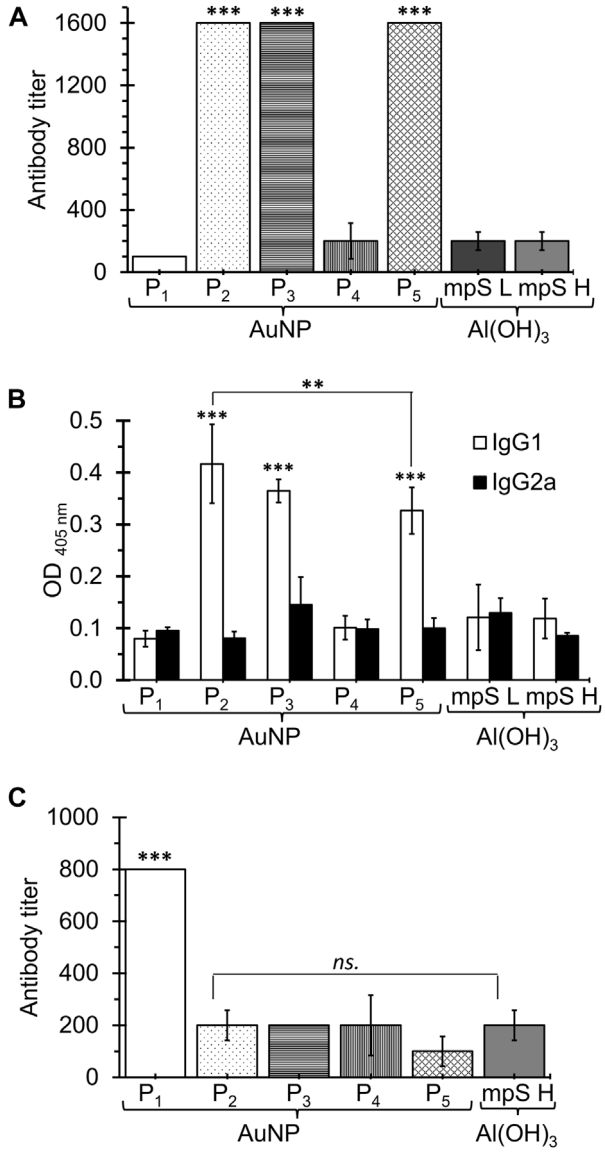

FIGURE 9
Anti-peptide IgG titers **(A)** and IgG1 and IgG2a serum levels **(B)** induced by immunization with the individual conjugates or with low-dose (5 μg) or high-dose (15 μg) HA adjuvant. Anti-Spike protein IgG titers induced by the individual conjugates or high-dose HA adjuvant **(C)**. Antibody titers were determined by ELISA on serial dilutions of test sera on day 45. Serum levels of IgG1 and IgG2a subclasses were determined by ELISA at a 1:200 dilution on day 45. Significance values were determined using two-way ANOVA with Turkey test. Significant differences are indicated as $*p < 0.05$, $**p < 0.01$, $***p < 0.001$, and non-significant differences as *ns*.

previous reports in which a greater toxic effect was observed after 48 h under AuNP-treatment of HeLa (Manivasagan and Oh, 2015), 1BR3, and A375 cells (Mioc et al., 2018). The cytotoxic effect of AuNP has been attributed to various factors such as particle size, dose, surface modification, and oxidative stress (Manivasagan and Oh, 2015). This last factor is influenced by the interaction of AuNP with biomolecules such as nucleic acids, proteins, and membrane lipids (Negahdary et al., 2015; Akhtar et al., 2012). A key factor in the antioxidant defense system and restoration of cell viability is intracellular glutathione concentration, which has been shown to delay cell death in pre-treated Hela and NHDF cells exposed to AuNP in the 0.028–100 μg/mL range (Akhtar et al., 2012; Lee et al., 2019). Although the performed *in vitro* assays allowed to justify the safety of the obtained conjugates, further studies will be aimed at elucidating the precise molecular mechanism involved in the cytotoxic effect observed in this study and how the intracellular processing of AuNP is managed once the nanomaterial has been internalized; also, evaluating the acute effects of the AuNP-based conjugates in the cells at the injection site is a relevant objective to better validate the safety of the proposed vaccine.

In terms of immunogenicity, the AuNP conjugates obtained induced higher antibody levels when compared to alum, especially AuNP-P_2, AuNP-P_3, and AuNP-P_5, with IgG antibody titers increased up to eight-fold higher and lasting up to 2 months after the last immunization. It is important to note that mice immunized with AuNP-P_2, AuNP-P_3, and AuNP-P_5 showed a marked predominance of the IgG1 subclass. This behavior in the IgG1/IgG2 ratio was similar to that observed in our previous work with peptide $S_{461\text{-}493}$ (Farfán-Castro et al., 2021), and is in agreement with previous reports where the polarization of the response towards the IgG1 subclass is attributed to the immunomodulatory properties of AuNP (Shinchi et al., 2019; Liu et al., 2021; Xu et al., 2021). In ELISA against the full-length protein S, lower IgG antibody titers were recorded when compared to the assays targeting the corresponding synthetic peptides. AuNP-P_1 was the only case showing a significant response, which was four-fold higher with respect to titers of the other groups. Surprisingly, such titers observed for AuNP-P_1 were eight-fold higher than those observed in the ELISA targeting the P_1 peptide, which could be attributed to a lower adsorption of the peptide to the surface of the well. Overall, these data suggest that AuNP-P_1 is effective at inducing functional antibodies capable of binding the native S protein. However, it is possible that the antibodies induced by AuNP-P_2, AuNP-P_3, and AuNP-P_5 could protect by recognizing the S protein in other conformations or mediate protection by other mechanisms different to viral entry blockade. One unexpected result is the inability of AuNP-P_1 and AuNP-P_4 conjugates to be immunogenic in mice, which could be associated to a deleterious effect of the coupling approach on the antigen display impeding the induction of humoral responses.

AuNP have been used as antigen carriers in several vaccines under development against a variety of pathogens. These nanovaccine candidates have generally produced positive immunological outcomes. Some mechanisms of activation of the immune system by AuNP include the activation of the NLRP3 inflammasome and secretion of related cytokines such as IL-1β and IL-18, as reported by Niikura et al. (2013) in bone-marrow-derived dendritic cells treated with gold nanorods coated with the West Nile virus envelope protein. AuNP have been shown to provide anti-inflammatory protection in macrophages by activating the Keap1/Nrf2 signaling pathway, and to induce NFkB signaling pathway in dendritic cells, which is related with their maturation and immune tolerance avoidance (Goldstein et al., 2016; Horwitz et al., 2021). In the present study, AuNP-PEG showed to enhance CD86 expression in the murine DC2.4 line, which suggests that one possible mechanism

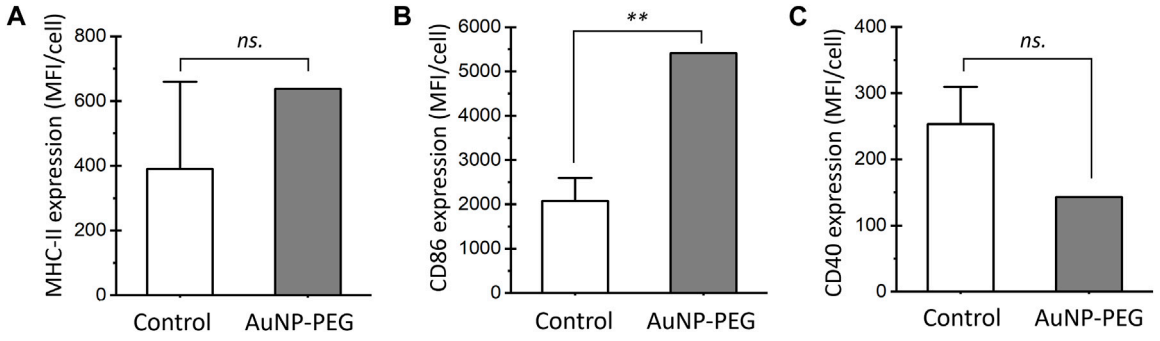

FIGURE 10
In vitro dendritic cell maturation assay. Expression of maturation markers MHC-II **(A)**, CD86 **(B)**, and CD40 **(C)** in DC2.4 cells that express CD11c. DCs were exposed for 24 h to 50 μg/mL of AuNP-PEG. The results are mean fluorescence intensity (MFI) values for each marker. Significance values were determined using two-way ANOVA with Turkey test. Significant differences are indicated as $^{**}p < 0.01$ and non-significant differences as *ns*.

explaining the adjuvant effect of this type of nanomaterial is their impact on DC maturation for a better antigen presentation. It has been described that DC undergo a complex maturation process which includes differences on the expression of the molecules of the major histocompatibility complex (MHC) and co-stimulatory molecules across the time (Macagno et al., 2007). This could be the reason for the differences found in the expression of CD86 and CD40 at the time of evaluation.

There are few vaccines against SARS-CoV-2 based on inorganic nanomaterials. An example is the AuNP-adjuvanted S protein vaccine tested in BALB/c mice (Sekimukai et al., 2020), which elicited a significant IgG response but could not mitigate eosinophilic infiltration due to the allergic inflammatory response. Kumar et al. (2021) also developed a gold-nanostar-chitosan DNA vaccine encoding the S protein against SARS-CoV-2 for intranasal immunization, which induced high levels of anti-SARS-CoV-2 IgA in lung mucosa, neutralization of pseudoviruses, and enhanced tissue-resident memory T cells.

Most vaccines need a cold chain to maintain the stability of the components during storage and distribution, until the immunogen is finally administered. Nevertheless, maintaining the cold chain can be difficult in locations with challenging access and involves monetary investment in refrigerated equipment. A benefit of AuNP-based vaccines is their thermal stability, even with temperature fluctuations, which reduces costs by eliminating the need for a cold chain. This is supported by the findings of Ingrole et al. (2021), who demonstrated that their lyophilized AuNP-based influenza A vaccine maintained its stability and immunogenicity for up to 3 months when stored at temperatures ranging from 4°C to 50°C, even when kept in its freeze-dried state and reconstituted in water. The reduced amount of antigen or adjuvants required in AuNP-based nanovaccines to elicit robust immune responses is another attractive feature of these platforms, and the surface antigens can be easily modified once the conjugation technique has been standardized.

It is important to expand the preclinical evaluation of the AuNP-$P_{1\text{-}5}$ conjugates under good laboratory practices and good manufacturing practices. In this regard, some of the most promissory are the naNO-DENGUE (NCT04935801) and naNO-COVID (NCT05113862) Phase-I clinical trials from Emergex Vaccines Holding Ltd., against Dengue and SARS-CoV-2, respectively. These vaccines consist of T-cells primed with specific cocktail of peptides from the respective viruses attached to AuNP. The naNO-COVID vaccine protected mice of lung inflammation after intranasal challenge with SARS-CoV-2 in preclinical studies (Emergex Vaccines, 2022). Ultimately, neutralization assays based on SARS-CoV-2 or pseudoviruses displaying the S protein are needed to ascertain the potential of these vaccine candidates. Moreover, assays to assess Fc-mediated phagocytosis and antibody-dependent cellular cytotoxicity could aid on determining additional mechanisms by which the obtained AuNP conjugates could result in immune protection against COVID-19 before evaluating these candidates in infectious challenge models.

In conclusion, this study expands the evidence on the potential of using AuNP as safe and effective carriers for nanovaccine design since the obtained AuNP-P_2, AuNP-P_3 and AuNP-P_5 conjugates did not induce irreversible *in vitro* cytotoxic effects and remarkably were able to induce robust and long-lasting antigen-specific IgG response in mice, with an IgG1 subclass predominance; surpassing the response induced by the conventional alum adjuvant. Moreover, the data obtained represent a step forward on the development of fully synthetic vaccines that could provide a solution for the need of thermostable vaccines targeting conserved regions from the S protein, with the potential to provide long-term and broad protection against SARS-CoV-2 VOC not depending on conventional adjuvants, which is a limitation for vaccine developers that has a priority to focus on formulations based on patent-free components.

Data availability statement

The original contributions presented in the study are included in the article/Supplementary Material, further inquiries can be directed to the corresponding authors.

Ethics statement

The animal study was approved by the Comité de Investigación y Docencia de la Facultad de Ciencias Químicas (approval number: CEID-2020-07R1). The study was conducted in accordance with the local legislation and institutional requirements.

Author contributions

SF-C: Formal Analysis, Investigation, Methodology, Writing–original draft. MG-S: Conceptualization, Data curation, Investigation, Methodology, Validation, Writing–review and editing. LB-M: Methodology, Validation, Writing–review and editing. JC: Methodology, Validation, Writing–review and editing. RS: Methodology, Validation, Writing–review and editing. OG-O: Conceptualization, Formal Analysis, Supervision, Writing–review and editing. SR-M: Conceptualization, Funding acquisition, Writing–original draft, Writing–review and editing.

Funding

The author(s) declare financial support was received for the research, authorship, and/or publication of this article. This research was funded by CONAHCYT (grant number 848290) and by PRODEP (grant UASLP-PTC-625).

Conflict of interest

The authors declare that the research was conducted in the absence of any commercial or financial relationships that could be construed as a potential conflict of interest.

Publisher's note

All claims expressed in this article are solely those of the authors and do not necessarily represent those of their affiliated organizations, or those of the publisher, the editors and the reviewers. Any product that may be evaluated in this article, or claim that may be made by its manufacturer, is not guaranteed or endorsed by the publisher.

Supplementary material

The Supplementary Material for this article can be found online at: https://www.frontiersin.org/articles/10.3389/fnano.2024.1335346/full#supplementary-material

References

Akhtar, M. J., Ahamed, M., Kumar, S., Khan, M. M., Ahmad, J., and Alrokayan, S. A. (2012). Zinc oxide nanoparticles selectively induce apoptosis in human cancer cells through reactive oxygen species. *Int. J. Nanomedicine* 7, 845–857. doi:10.2147/IJN.S29129

Amrun, S. N., Lee, C.Y.-P., Lee, B., Fong, S.-W., Young, B. E., Chee, R.S.-L., et al. (2020). Linear B-cell epitopes in the spike and nucleocapsid proteins as markers of SARS-CoV-2 exposure and disease severity. *EBioMedicine* 58, 102911. doi:10.1016/j.ebiom.2020.102911

Bartczak, D., and Kanaras, A. G. (2011). Preparation of peptide-functionalized gold nanoparticles using one pot EDC/Sulfo-NHS coupling. *Langmuir* 27 (16), 10119–10123. doi:10.1021/la2022177

Bekić, M., Tomić, S., Rudolf, R., Milanović, M., Vučević, D., Anžel, I., et al. (2019). The effect of stabilisation agents on the immunomodulatory properties of gold nanoparticles obtained by ultrasonic spray pyrolysis. *Mater. (Basel, Switz.* 12 (24), 4121–4215. doi:10.3390/MA12244121

Callaway, E. (2020). The race for coronavirus vaccines: a graphical guide. *Nature* 580 (7805), 576–577. doi:10.1038/d41586-020-01221-y

Chen, H., Paholak, H., Ito, M., Sansanaphongpricha, K., Qian, W., Che, Y., et al. (2013). Living PEGylation on gold nanoparticles to optimize cancer cell uptake by controlling targeting ligand and charge densities. *Nanotechnology* 24 (1-9), 355101. doi:10.1088/0957-4484/24/35/355101

Cheng, L., Zhu, G., Liu, G., and Zhu, L. (2020). FDTD simulation of the optical properties for gold nanoparticles. *Mater. Res. Express* 7 (12), 125009. doi:10.1088/2053-1591/abd139

Chung, J. Y., Thone, M. N., and Kwon, Y. J. (2021). COVID-19 vaccines: the status and perspectives in delivery points of view. *Adv. Drug Deliv. Rev.* 170, 1–25. doi:10.1016/j.addr.2020.12.011

Climent, N., García, I., Marradi, M., Chiodo, F., Miralles, L., Maleno, M. J., et al. (2018). Loading dendritic cells with gold nanoparticles (GNPs) bearing HIV-peptides and mannosides enhance HIV-specific T cell responses. *Nanomedicine Nanotechnol. Biol. Med.* 14 (2), 339–351. doi:10.1016/j.nano.2017.11.009

CoVariants (2020). Available at: https://covariants.org/ (Accessed October 17, 2023).

Cruje, C., and Chithrani, D. B. (2014). Polyethylene glycol functionalized nanoparticles for improved cancer treatment. *Rev. Nanosci. Nanotechnol.* 3 (1), 20–30. doi:10.1166/rnn.2014.1042

Dai, L., and Gao, G. F. (2021). Viral targets for vaccines against COVID-19. *Nat. Rev. Immunol.* 21, 73–82. doi:10.1038/s41577-020-00480-0

Das, J., Choi, Y.-J., Yasuda, H., Han, J. W., Park, C., Song, H., et al. (2016). Efficient delivery of C/EBP beta gene into human mesenchymal stem cells via polyethylenimine-coated gold nanoparticles enhances adipogenic differentiation. *Sci. Rep.* 6 (1), 33784. doi:10.1038/srep33784

Dykman, L. A., Staroverov, S. A., Fomin, A. S., Khanadeev, V. A., Khlebtsov, B. N., and Bogatyrev, V. A. (2018). Gold nanoparticles as an adjuvant: influence of size, shape, and technique of combination with CpG on antibody production. *Int. Immunopharmacol.* 54, 163–168. doi:10.1016/j.intimp.2017.11.008

EMA (2021). *Regulatory requirements for vaccines intended to provide protection against variant strain(s) of SARS-CoV-2 - scientific guideline*. Ene. European Medicines Agency. Amsterdan, Netherlands. Available at: https://www.ema.europa.eu/en/regulatory-requirements-vaccines-intended-provide-protection-against-variant-strains-sars-cov-2 (Accessed 23, 2023).

Emergex Vaccines (2022). Emergex provides an update on first-in-human studies of its novel Dengue fever and coronavirus T cell adaptive vaccines. Available at: https://emergexvaccines.com/emergex-provides-an-update-on-first-in-human-studies-of-its-novel-dengue-fever-and-coronavirus-t-cell-adaptive-vaccines/ (Accessed October 17, 2023).

Escareno, N., Topete, A., Taboada, P., and Daneri-Navarro, A. (2018). Rational surface engineering of colloidal Drug delivery systems for biological applications. *Curr. Top. Med. Chem.* 18 (14), 1224–1241. doi:10.2174/1568026618666180810145234

Farfán-Castro, S., García-Soto, M. J., Comas-García, M., Arévalo-Villalobos, J. I., Palestino, G., González-Ortega, O., et al. (2021). Synthesis and immunogenicity assessment of a gold nanoparticle conjugate for the delivery of a peptide from SARS-CoV-2. *Nanomedicine Nanotechnol. Biol. Med.* 34, 102372. doi:10.1016/j.nano.2021.102372

Favi, P. M., Gao, M., Johana Sepúlveda Arango, L., Ospina, S. P., Morales, M., Pavon, J. J., et al. (2015). Shape and surface effects on the cytotoxicity of nanoparticles: gold nanospheres versus gold nanostars. *J. Biomed. Mater. Res. Part A* 103 (11), 3449–3462. doi:10.1002/jbm.a.35491

Foroozandeh, P., and Aziz, A. A. (2018). Insight into cellular uptake and intracellular trafficking of nanoparticles. *Nanoscale Res. Lett.* 13 (1), 339. doi:10.1186/s11671-018-2728-6

Ghafari, M., Watson, O. J., Karlinsky, A., Ferretti, L., and Katzourakis, A. (2022). A framework for reconstructing SARS-CoV-2 transmission dynamics using excess mortality data. *Nat. Commun.* 13 (1), 3015. doi:10.1038/s41467-022-30711-y

Goldstein, A., Soroka, Y., Frušić-Zlotkin, M., Lewis, A., and Kohen, R. (2016). The bright side of plasmonic gold nanoparticles; activation of Nrf2, the cellular protective pathway. *Nanoscale* 8 (22), 11748–11759. doi:10.1039/c6nr02113a

Gulla, S. K., Rao, B. R., Moku, G., Jinka, S., Nimmu, N. V., Khalid, S. H., et al. (2019). In vivotargeting of DNA vaccines to dendritic cells using functionalized gold nanoparticles. *Biomaterials Sci.* 7 (3), 773–788. doi:10.1039/c8bm01272e

Haiss, W., Thanh, N. T. K., Aveyard, J., and Fernig, D. G. (2007). Determination of size and concentration of gold nanoparticles from UV−Vis spectra. *Anal. Chem.* 79 (11), 4215–4221. doi:10.1021/ac0702084

Heffron, A. S., McIlwain, S. J., Amjadi, M. F., Baker, D., Khullar, S., Sethi, A. K., et al. (2020). *The landscape of antibody binding in SARS-CoV-2 infection*. Cold Spring Harbor Laboratory. Long Island, New York. bioRxiv. doi:10.1101/2020.10.10.334292

Hermanson, G. T. (2013). *Bioconjugate techniques*. Amsterdam: Acad. Press.

Horwitz, D. A., Bickerton, S., and La Cava, A. (2021). Strategies to use nanoparticles to generate CD4 and CD8 regulatory T cells for the treatment of SLE and other autoimmune diseases. *Front. Immunol.* 12, 681062. doi:10.3389/fimmu.2021.681062

Ibrahim, N. A., Nada, A. A., and Eid, B. M. (2018). "Polysaccharide-based polymer gels and their potential applications," in *Polymer gels. Gels horizons: from science to Smart materials* (Singapore: Springer). doi:10.1007/978-981-10-6083-0_4

Ingrole, R. S. J., Tao, W., Joshi, G., and Gill, H. S. (2021). M2e conjugated gold nanoparticle influenza vaccine displays thermal stability at elevated temperatures and confers protection to ferrets. *Vaccine* 39 (34), 4800–4809. doi:10.1016/j.vaccine.2021.07.032

Johnson, P. B., and Christy, R. W. (1972). Optical constants of the noble metals. *Phys. Rev. B* 6 (12), 4370–4379. doi:10.1103/physrevb.6.4370

Kang, Y.-F., Sun, C., Zhuang, Z., Yuan, R.-Y., Zheng, Q., Li, J.-P., et al. (2021). Rapid development of SARS-CoV-2 spike protein receptor-binding domain self-assembled nanoparticle vaccine candidates. *ACS Nano* 15 (2), 2738–2752. doi:10.1021/acsnano.0c08379

Krishnamoorthy, S., Swain, B., Verma, R. S., and Gunthe, S. S. (2020). SARS-CoV, MERS-CoV, and 2019-nCoV viruses: an overview of origin, evolution, and genetic variations. *VirusDisease* 31, 411–423. doi:10.1007/s13337-020-00632-9

Kumar, U. S., Afjei, R., Ferrara, K., Massoud, T. F., and Paulmurugan, R. (2021). Gold-nanostar-chitosan-mediated delivery of SARS-CoV-2 DNA vaccine for respiratory mucosal immunization: development and proof-of-principle. *ACS Nano* 15 (11), 17582–17601. doi:10.1021/acsnano.1c05002

Lee, E., Jeon, H., Lee, M., Ryu, J., Kang, C., Kim, S., et al. (2019). Molecular origin of AuNPs-induced cytotoxicity and mechanistic study. *Sci. Rep.* 9 (1), 2494. doi:10.1038/s41598-019-39579-3

Li, L., Zhao, Z., Yang, X., Li, W., Chen, S., Sun, T., et al. (2020). *Identification of four linear B-cell epitopes on the SARS-CoV-2 spike protein able to elicit neutralizing antibodies. bioRxiv*. Long Island, New York. Cold Spring Harbor Laboratory. doi:10.1101/2020.12.13.422550

Li, Y., Jin, Q., Ding, P., Zhou, W., Chai, Y., Li, X., et al. (2020). Gold nanoparticles enhance immune responses in mice against recombinant classical swine fever virus E2 protein. *Biotechnol. Lett.* 42 (7), 1169–1180. doi:10.1007/s10529-020-02853-w

Liu, F., Vander Elst, L., Müller, R. N., and Laurent, S. (2018). Structure of CoFe2O4@CdTe nanocomposite with core/shell structure for high-performance Bi-modal imaging. *Colloids Surfaces A Physicochem. Eng. Aspects* 538, 467–473. doi:10.1016/j.colsurfa.2017.10.081

Liu, Y., Wang, Z., Fan, Y., Li, M., Zhu, H., Wang, K., et al. (2021). The adjuvant of α-galactosylceramide presented by gold nanoparticles enhances antitumor immune responses of MUC1 antigen-based tumor vaccines. *Int. J. Nanomedicine* 16, 403–420. doi:10.2147/ijn.s273883

Lu, J., Xue, Y., Shi, R., Kang, J., Zhao, C.-Y., Zhang, N.-N., et al. (2019). A non-sacrificial method for the quantification of poly(ethylene glycol) grafting density on gold nanoparticles for applications in nanomedicine. *Chem. Sci.* 10 (7), 2067–2074. doi:10.1039/c8sc02847h

Macagno, A., Napolitani, G., Lanzavecchia, A., and Sallusto, F. (2007). Duration, combination and timing: the signal integration model of dendritic cell activation. *Trends Immunol.* 28 (5), 227–233. doi:10.1016/j.it.2007.03.008

Manivasagan, P., and Oh, J. (2015). Production of a novel fucoidanase for the green synthesis of gold nanoparticles by streptomyces sp. and its cytotoxic effect on HeLa cells. *Mar. Drugs* 13 (11), 6818–6837. doi:10.3390/md13116818

Marcilla, A., Gómez-Siurana, A., Beltrán, M., Martínez-Castellanos, I., Blasco, I., and Berenguer, D. (2018). TGA-FTIR study of the pyrolysis of sodium citrate and its effect on the pyrolysis of tobacco and tobacco/SBA-15 mixtures under N2 and air atmospheres. *J. Sci. Food Agric.* 98 (15), 5916–5931. doi:10.1002/jsfa.9121

Maurel, M., Montheil, T., Martin, J., Chaar, L., Guzman-Gonzalez, V., Couvet, M., et al. (2021). Design of PEGylated three ligands silica nanoparticles for multi-receptor targeting. *Nanomaterials* 11 (1), 177. doi:10.3390/nano11010177

McLean, G., Kamil, J., Lee, B., Moore, P., Schulz, T. F., Muik, A., et al. (2022). The impact of evolving SARS-CoV-2 mutations and variants on COVID-19 vaccines. *mBio* 13 (2), e0297921. doi:10.1128/mbio.02979-21

Meka, R. R., Mukherjee, S., Patra, C. R., and Chaudhuri, A. (2019). Shikimoyl-ligand decorated gold nanoparticles for use in *ex vivo* engineered dendritic cell based DNA vaccination. *Nanoscale* 11 (16), 7931–7943. doi:10.1039/c8nr10293g

Mioc, M., Pavel, I. Z., Ghiulai, R., Coricovac, D. E., Farcaş, C., Mihali, C.-V., et al. (2018). The cytotoxic effects of betulin-conjugated gold nanoparticles as stable formulations in normal and melanoma cells. *Front. Pharmacol.* 9, 429. doi:10.3389/fphar.2018.00429

Mironava, T., Hadjiargyrou, M., Simon, M., Jurukovski, V., and Rafailovich, M. H. (2010). Gold nanoparticles cellular toxicity and recovery: effect of size, concentration and exposure time. *Nanotoxicology* 4 (1), 120–137. doi:10.3109/17435390903471463

Negahdary, M., Reyhaneh, C., Shahrzad, K. Z., and Marziyeh, A. (2015). The antioxidant effects of silver, gold, and zinc oxide nanoparticles on male mice in *in vivo* condition. *Adv. Biomed. Res.* 4 (69), 69. doi:10.4103/2277-9175.153893

Ng, K. W., Faulkner, N., Finsterbusch, K., Wu, M., Harvey, R., Hussain, S., et al. (2022). SARS-CoV-2 S2–targeted vaccination elicits broadly neutralizing antibodies. *Sci. Transl. Med.* 14 (655), eabn3715. doi:10.1126/scitranslmed.abn3715

Niikura, K., Matsunaga, T., Suzuki, T., Kobayashi, S., Yamaguchi, H., Orba, Y., et al. (2013). Gold nanoparticles as a vaccine platform: influence of size and shape on immunological responsesin vitroand*in vivo*. *ACS Nano* 7 (5), 3926–3938. doi:10.1021/nn3057005

Perry, J. L., Reuter, K. G., Kai, M. P., Herlihy, K. P., Jones, S. W., Luft, J. C., et al. (2012). PEGylated PRINT nanoparticles: the impact of PEG density on protein binding, macrophage association, biodistribution, and pharmacokinetics. *Nano Lett.* 12 (10), 5304–5310. doi:10.1021/nl302638g

Pinto, D., Sauer, M. M., Czudnochowski, N., Low, J. S., Tortorici, M. A., Housley, M. P., et al. (2021). Broad betacoronavirus neutralization by a stem helix–specific human antibody. *Science* 373 (6559), 1109–1116. doi:10.1126/science.abj3321

Poh, C. M., Carissimo, G., Wang, B., Amrun, S. N., Lee, C.Y.-P., Chee, R.S.-L., et al. (2020). Two linear epitopes on the SARS-CoV-2 spike protein that elicit neutralising antibodies in COVID-19 patients. *Nat. Commun.* 11 (1), 2806. doi:10.1038/s41467-020-16638-2

Qian, T., Li, J., Feng, W., and Nian, H. (2017). Enhanced thermal conductivity of form-stable phase change composite with single-walled carbon nanotubes for thermal energy storage. *Sci. Rep.* 7 (1), 44710. doi:10.1038/srep44710

Raghuwanshi, D., Mishra, V., Das, D., Kaur, K., and Suresh, M. R. (2012). Dendritic cell targeted chitosan nanoparticles for nasal DNA immunization against SARS CoV nucleocapsid protein. *Mol. Pharm.* 9 (4), 946–956. doi:10.1021/mp200553x

Rahme, K., Chen, L., Hobbs, R. G., Morris, M. A., O'Driscoll, C., and Holmes, J. D. (2013). PEGylated gold nanoparticles: polymer quantification as a function of PEG lengths and nanoparticle dimensions. *RSC Adv.* 3 (17), 6085–6094. doi:10.1039/c3ra22739a

Sekimukai, H., Iwata-Yoshikawa, N., Fukushi, S., Tani, H., Kataoka, M., Suzuki, T., et al. (2020). Gold nanoparticle-adjuvanted S protein induces a strong antigen-specific IgG response against severe acute respiratory syndrome-related coronavirus infection but fails to induce protective antibodies and limit eosinophilic infiltration in lungs. *Microbiol. Immunol.* 64 (1), 33–51. doi:10.1111/1348-0421.12754

Shardlow, E., Mold, M., and Exley, C. (2018). Unraveling the enigma: elucidating the relationship between the physicochemical properties of aluminium-based adjuvants and their immunological mechanisms of action. *Allergy, Asthma and Clin. Immunol.* 14 (1), 80. doi:10.1186/s13223-018-0305-2

Shinchi, H., Yamaguchi, T., Moroishi, T., Yuki, M., Wakao, M., Cottam, H. B., et al. (2019). Gold nanoparticles coimmobilized with small molecule toll-like receptor 7 ligand and α-mannose as adjuvants. *Bioconjugate Chem.* 30 (11), 2811–2821. doi:10.1021/acs.bioconjchem.9b00560

Shukla, R., Bansal, V., Chaudhary, M., Basu, A., Bhonde, R. R., and Sastry, M. (2005). Biocompatibility of gold nanoparticles and their endocytotic fate inside the cellular compartment: a microscopic overview. *Langmuir* 21 (23), 10644–10654. doi:10.1021/la0513712

Tapia, D., Sanchez-Villamil, J. I., Stevenson, H. L., and Torres, A. G. (2021). Multicomponent gold-linked glycoconjugate vaccine elicits antigen-specific humoral and mixed TH1-TH17 immunity, correlated with increased protection against burkholderia pseudomallei. *MBio* 12 (3), e0122721. doi:10.1128/mbio.01227-21

Tomić, S., Đokić, J., Vasilijić, S., Ogrinc, N., Rudolf, R., Pelicon, P., et al. (2014). Size-dependent effects of gold nanoparticles uptake on maturation and antitumor functions of human dendritic cells *in vitro*. *PLoS ONE* 9 (5), e96584. doi:10.1371/journal.pone.0096584

Trabbic, K. R., Kleski, K. A., and Barchi, J. J. (2021). Stable gold-nanoparticle-based vaccine for the targeted delivery of tumor-associated glycopeptide antigens. *ACS Bio Med Chem Au* 1 (1), 31–43. doi:10.1021/acsbiomedchemau.1c00021

U.S. Food and Drug Administration (2021). Emergency use authorization for vaccines to prevent COVID-19: guidance for industry. Available at: https://www.fda.gov/regulatory-information/search-fda-guidance-documents/emergency-use-authorization-vaccines-prevent-covid-19 (Accessed September 15, 2023).

Vasquez, Y., Kolle, M., Mishchenko, L., Hatton, B. D., and Aizenberg, J. (2014). Three-phase Co-assembly: *in situ* incorporation of nanoparticles into tunable, highly ordered, porous silica films. *ACS Photonics* 1 (1), 53–60. doi:10.1021/ph400067z

Wang, C., Zhu, W., and Wang, B.-Z. (2017). Dual-linker gold nanoparticles as adjuvanting carriers for multivalent display of recombinant influenza hemagglutinin trimers and flagellin improve the immunological responses *in vivo* and *in vitro*. *Int. J. Nanomedicine* 12, 4747–4762. doi:10.2147/ijn.s137222

Wang, W., Wei, Q., Wang, J., Wang, B., Zhang, S., and Yuan, Z. (2013). Role of thiol-containing polyethylene glycol (thiol-PEG) in the modification process of gold nanoparticles (AuNPs): stabilizer or coagulant? *J. colloid interface Sci.* 404, 223–229. doi:10.1016/j.jcis.2013.04.020

World Health Organization (2023). *WHO COVID-19 dashboard*. Geneva, Switzerland. World Health Organization. Available at: https://covid19.who.int/ (Accessed September 15, 2023).

Xu, X., Gan, M., Ge, Y., Cheng, Y., Feng, T., Liu, M., et al. (2021). Multifaceted glycoadjuvant@AuNPs inhibits tumor metastasis through promoting T cell activation and remodeling tumor microenvironment. *J. Nanobiotechnology* 19 (1), 376. doi:10.1186/s12951-021-01129-3

Zhang, X. (2015). Gold nanoparticles: recent advances in the biomedical applications. *Cell Biochem. Biophysics* 72 (3), 771–775. doi:10.1007/s12013-015-0529-4

Zhou, Q., Zhang, Y., Du, J., Li, Y., Zhou, Y., Fu, Q., et al. (2016). Different-sized gold nanoparticle activator/antigen increases dendritic cells accumulation in liver-draining lymph nodes and CD8+ T cell responses. *ACS Nano* 10 (2), 2678–2692. doi:10.1021/acsnano.5b07716